The fictitious domain method and applications in wave propagation

Eliane Bécache, Jerónimo Rodríguez Garcia, Chrysoula Tsogka

COMPDYN 2009
ECCOMAS Thematic Conference on
Computational Methods in Structural Dynamics and Earthquake Engineering
M. Papadrakakis, N.D. Lagaros, M. Fragiadakis (eds.)
Rhodes, Greece, 22-24 June 2009

THE FICTITIOUS DOMAIN METHOD AND APPLICATIONS IN WAVE PROPAGATION

Éliane Bécache[1], Jeronimo Rodriguez[2], and Chrysoula Tsogka[3]

[1]POEMS, INRIA-Rocquencourt
BP 105, 78153 Le Chesnay Cedex, France
e-mail: eliane.becache@inria.fr

[2] Dept. of Applied Mathematics,
Univ. Santiago de Compostela
15782 Santiago de Compostela, Spain
e-mail: jeronimo.rodriguez@ensta.fr

[3]IACM-FORTH
PO BOX 1385, Vassilika Vouton, 71110 Heraklion, Greece
e-mail:tsogka@tem.uoc.gr

Keywords: fictitious domain method, mixed finite elements, cracks, elastic waves, acoustic waves

Abstract. *This paper deals with the convergence analysis of the fictitious domain method used for taking into account the Neumann boundary condition on the surface of a crack (or more generally an object) in the context of acoustic and elastic wave propagation. For both types of waves we consider the first order in time formulation of the problem known as mixed velocity-pressure formulation for acoustics and velocity-stress formulation for elastodynamics. The convergence analysis for the discrete problem depends on the mixed finite elements used. We consider here two families of mixed finite elements that are compatible with mass lumping. When using the first one which is less expensive and corresponds to the choice made in a previous paper, it is shown that the fictitious domain method does not always converge. For the second one a theoretical convergence analysis was carried out in [7] for the acoustic case. Here we present numerical results that illustrate the convergence of the method both for acoustic and elastic waves.*

1 Introduction

This work falls within the more general framework of developing efficient numerical methods for approximating wave propagation in complex media such as anisotropic, heterogeneous media with cracks or objects of arbitrary shapes. We consider here scattering of acoustic and elastic waves by perfect reflectors, *i.e.*, objects or cracks with a homogeneous Neumann boundary condition. To solve these wave propagation problems in an efficient way we use a fictitious domain approach. This approach, also called the domain embedding method, consists in extending artificially the solution inside the object so that the new domain of computation has a very simple shape (typically a rectangle in 2D). To account for the boundary condition, a new auxiliary unknown, defined only at the boundary of the object, is introduced. The solution of this extended problem has now a singularity across the boundary of the object which can be related to the new unknown. The main advantage of the method is that the mesh for the solution on the enlarged domain can be chosen independently of the geometry of the object. In particular, one can use regular grids or structured meshes which allows for simple and efficient computations.

Special interest has been given to this approach as it has been shown to lead to efficient numerical methods for a large number of applications (e.g [1, 19, 13, 12, 14, 16, 17]) and these last years for time dependent wave propagation problems ([9, 11, 21, 18, 5, 2]). The method can be re-interpreted in terms of optimization theory in which case the auxiliary unknown appears as a Lagrange multiplier associated to the boundary condition viewed now as an equality constraint in the functional space. Thus the key point of the approach is that it can be applied to essential type boundary conditions, *i.e.*, conditions that can be considered as an equality constraint.

To do so with the free surface condition, the dual unknown (velocity in the acoustic case and stress tensor in the elastic) has to be one of the unknowns. This can be done by considering either the dual formulation (the formulation with only one unknown, the dual one) or the mixed dual primal formulation. In both cases, the dual unknown is introduced and seeked for in the space $H(\mathrm{div})$ in which the Neumann boundary condition $\mathbf{v} \cdot n$ or $\boldsymbol{\sigma} \cdot n = 0$ can be considered as an equality constraint. In this case, the Lagrange multiplier is nothing but the jump of the primal unknown across the boundary of the object.

For the approximation of the mixed formulation in the scalar acoustic case, in [4], the authors have proposed mixed finite elements, the so-called $Q_{k+1}^{div} - Q_k$ elements, inspired by Nédélec's second family [20]. These elements are compatible with mass lumping, and therefore allow for constructing explicit schemes in time. The generalization of those elements in the case of elastic waves was introduced in [3] for the velocity-stress formulation.

A non standard convergence analysis of the $Q_{k+1}^{div} - Q_k$ elements has been carried out in [4] for their scalar version and in [6] for their elastodynamic vectorial version. However this convergence analysis only deals with the velocity-pressure (resp. velocity-stress) mixed problem without object, that is, it did not concern the convergence of the fictitious domain method.

In this paper the convergence of the fictitious domain method is analyzed. The scalar problem is considered first, followed by the vectorial elastic case.

2 The fictitious domain formulation of the diffraction problem. The acoustic case

2.1 The continuous problem

We consider the diffraction of an acoustic wave by an object with a Neumann type condition for the pressure field on its boundary Γ. The object can be either an obstacle with a closed boundary or a crack with an open boundary (see Fig. 1) but for the sake of clarity we will

consider here only this second configuration. The domain of propagation is denoted Ω with an exterior boundary Σ (see Fig. 1) and we assume that $C = \Omega \cup \Gamma$ is a domain of "simple" geometry, typically a rectangle. The propagation medium is assumed to be anisotropic and

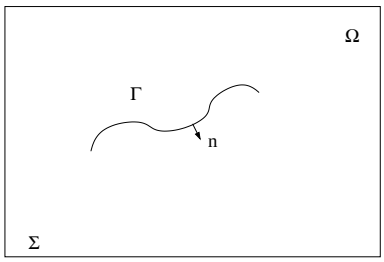

Figure 1: Geometry of the problem.

the equation satisfied by the pressure field is the scalar wave equation. To apply the fictitious domain method to this type of boundary condition it is classical (e.g. [4]) to formulate the problem as a first-order velocity-pressure system,

$$\left\{\begin{array}{l} \text{Find } (\mathbf{v},p) : (x,t) \in \Omega \times [0,T] \mapsto (\mathbf{v}(x,t),p(x,t)) \in \mathbb{R}^2 \times \mathbb{R} \text{ satisfying,} \\ \rho\dfrac{\partial p}{\partial t} - \text{div } \mathbf{v} = f, \quad \text{in } \Omega, \quad (a) \\ \mathbf{A}\dfrac{\partial \mathbf{v}}{\partial t} - \nabla p = 0, \quad \text{in } \Omega, \quad (b) \\ \mathbf{v}\cdot n = 0, \quad \text{on } \Gamma, \quad (c) \\ p = 0, \quad \text{on } \Sigma, \quad (d) \end{array}\right. \tag{1}$$

with the initial conditions,

$$\left\{\begin{array}{lll} p(t=0) & = & p_0, \\ \mathbf{v}(t=0) & = & \mathbf{v}_0, \end{array}\right. \tag{2}$$

where the unknowns p and $\mathbf{v}$ denote the pressure and the velocity field. The scalar function ρ and the tensor $\mathbf{A}$ characterize the propagation medium and f represents the external forces. Moreover, we assume that ρ satisfies

$$0 < \rho^- \leq \rho(x) \leq \rho^+ < +\infty,$$

and $\mathbf{A}$ is a second order symmetric positive tensor such that

$$0 < \kappa|\mathbf{w}|^2 \leq \mathbf{A}(x)\mathbf{w}\cdot\mathbf{w} \leq \nu|\mathbf{w}|^2, \quad \forall \mathbf{w} \neq 0.$$

We also assume that the support of the initial data and the source do not intersect Γ,

$$\text{supp}(\mathbf{v}_0) \cup \text{supp}(p_0) \subset C \setminus \Gamma, \quad \bigcup_{t\leq T} \text{supp}(f(t)) \subset C \setminus \Gamma. \tag{3}$$

The *natural* variational formulation of this problem would be set in some functional spaces that depend on the shape of the obstacle (i.e., depend on Ω). More precisely, the classical variational

formulation is,

$$\left\{\begin{array}{l} \text{Find } (\mathbf{v}(t),p(t)) \in \underline{X}_0 \times M \text{ satisfying,} \\ \dfrac{\mathrm{d}}{\mathrm{d}t}\displaystyle\int_\Omega \mathbf{A}\mathbf{v}\cdot\mathbf{w}\,\mathrm{d}x \;+\; \int_\Omega \mathrm{div}(\mathbf{w})p\,\mathrm{d}x \;=\; 0, \qquad \forall \mathbf{w}\in \underline{X}_0, \\ \dfrac{\mathrm{d}}{\mathrm{d}t}\displaystyle\int_\Omega \rho p q\,\mathrm{d}x \;-\; \int_\Omega \mathrm{div}(\mathbf{v})q\,\mathrm{d}x \;=\; (f,q), \quad \forall q\in M, \\ (\mathbf{v},p)_{/t=0} \;=\; (\mathbf{v}_0,p_0), \end{array}\right. \tag{4}$$

where the functional spaces are defined as,

$$\underline{X}_0 = \{\mathbf{w}\in H(\mathrm{div};\Omega),\ \mathbf{w}\cdot\mathbf{n}=0,\ \text{ on } \Gamma\}\,,\ M = L^2(\Omega).$$

The fictitious domain formulation of this problem consists in taking into account the boundary condition on Γ in a weak way, by introducing a Lagrange multiplier λ defined on Γ. This allows for working in functional spaces (for the volume unknowns) which do not depend any more on the shape of the obstacle. The fictitious domain formulation is then the following, (to simplify the notations, we still denote by $(\mathbf{v}(t),p(t))$ the new unknowns defined now in C)

$$\left\{\begin{array}{l} \text{Find } (\mathbf{v}(t),p(t),\lambda(t)) \in \underline{X}\times M\times \mathcal{G} \text{ satisfying,} \\ \dfrac{\mathrm{d}}{\mathrm{d}t}a(\mathbf{v},\mathbf{w}) \;+\; b(\mathbf{w},p) \;-\; <\mathbf{w}\cdot\mathbf{n},\lambda>_\Gamma \;=\; 0, \qquad \forall \mathbf{w}\in\underline{X}, \\ \dfrac{\mathrm{d}}{\mathrm{d}t}(p,q)_\rho \;-\; b(\mathbf{v},q) \;=\; (f,q), \quad \forall q\in M, \\ \qquad\qquad <\mathbf{v}\cdot\mathbf{n},\mu>_\Gamma \;=\; 0, \qquad \forall \mu\in\mathcal{G}, \\ (\mathbf{v},p)_{/t=0} \;=\; (\mathbf{v}_0,p_0), \end{array}\right. \tag{5}$$

where the functional spaces are now defined as,

$$\underline{X}(=\underline{X}(C)) = H(\mathrm{div};C),\ M = L^2(C),\ \mathcal{G} = H^{1/2}_{00}(\Gamma),$$

the bilinear forms as,

$$\left\{\begin{array}{lll} a(\mathbf{v},\mathbf{w}) &=& \displaystyle\int_C \mathbf{A}\mathbf{v}\cdot\mathbf{w}\,\mathrm{d}x, \quad \forall(\mathbf{v},\mathbf{w})\in\underline{X}\times\underline{X}, \\ (p,q)_\eta &=& \displaystyle\int_C \eta\, p\, q\,\mathrm{d}x, \qquad \forall(p,q)\in M\times M, \\ b(\mathbf{w},q) &=& \displaystyle\int_C \mathrm{div}(\mathbf{w})q\,\mathrm{d}x, \quad \forall(\mathbf{w},q)\in\underline{X}\times M, \end{array}\right. \tag{6}$$

and the bracket $<\mathbf{w}\cdot\mathbf{n},\mu>_\Gamma$ is the duality product between $\mathcal{G}$ and $\mathcal{G}'$. In the following we will denote by $(\cdot,\cdot) := (\cdot,\cdot)_1$ the usual $L^2(C)$ scalar product.

Remark 1 On the regularity of the solution. *The space regularity of the volumic part of the solution is at most,*

$$\mathbf{v}(t)\ \in\ H^{\frac{1}{2}-\varepsilon}(\mathrm{div},C), \quad p(t)\in H^{\frac{1}{2}-\varepsilon}(C), \qquad \varepsilon>0,$$

and this is obtained for regular enough data and a regular geometry of the crack. The regularity in Ω (i.e. outside the obstacle) is in general higher and depends on the geometry of the obstacle. For a closed boundary we have,

$$p_{/\Omega}(t)\in H^2(\Omega), \quad \lambda(t)\in H^{3/2}(\Gamma)$$

While for an open boundary, due to the singular behavior near the tip of the crack [15] (the solution behaves as $\sqrt{r}$, r being here the distance to the tip), we have

$$p_{/\Omega}(t) \in H^{3/2-\varepsilon}(\Omega), \quad \lambda(t) \in H^{1-\varepsilon}(\Gamma), \qquad \varepsilon > 0.$$

2.2 The semi-discrete approximation

For the approximation in space of this problem, we introduce finite dimensional spaces $\underline{X_h} \subset \underline{X}$, $M_h \subset M$ and $\mathcal{G}_H \subset \mathcal{G}$ satisfying the approximation properties,

$$\left| \begin{array}{lcll} \lim\limits_{h\to 0} \inf\limits_{\mathbf{w}_h \in \underline{X_h}} \|\mathbf{v} - \mathbf{w}_h\|_{\underline{X}} & = & 0, & \forall \mathbf{v} \in \underline{X}, \\ \lim\limits_{h\to 0} \inf\limits_{q_h \in M_h} \|p - q_h\|_M & = & 0, & \forall p \in M, \\ \lim\limits_{H\to 0} \inf\limits_{\mu_H \in \mathcal{G}_H} \|\lambda - \mu_H\|_{\mathcal{G}} & = & 0, & \forall \lambda \in \mathcal{G}. \end{array} \right. \tag{7}$$

The semi-discrete problem is then,

$$\left\{ \begin{array}{l} \text{Find } (\mathbf{v}_h(t), p_h(t), \lambda_H(t)) \in \underline{X_h} \times M_h \times \mathcal{G}_H \text{ such that,} \\ \dfrac{\mathrm{d}}{\mathrm{d}t} a(\mathbf{v}_h, \mathbf{w}_h) + b(\mathbf{w}_h, p_h) - < \mathbf{w}_h \cdot \mathbf{n}, \lambda_H >_\Gamma = 0, \qquad \forall \mathbf{w}_h \in \underline{X_h}, \\ \dfrac{\mathrm{d}}{\mathrm{d}t} (p_h, q_h)_\rho - b(\mathbf{v}_h, q_h) = (f, q_h), \quad \forall q_h \in M_h, \\ \qquad\qquad < \mathbf{v}_h \cdot \mathbf{n}, \mu_H >_\Gamma = 0, \qquad \forall \mu_H \in \mathcal{G}_H, \\ \mathbf{v}_h(t=0) = \mathbf{v}_{h,0}, \\ p_h(t=0) = p_{h,0}, \end{array} \right. \tag{8}$$

where $(\mathbf{v}_{h,0}, p_{h,0}) \in X_h \times M_h$ is an approximation of the exact initial condition.

The question is : how to choose the approximate spaces in order to insure the convergence of $(\mathbf{v}_h, p_h, \lambda_H)$ to $(\mathbf{v}, p, \lambda)$?

3 The fictitious domain method using the $Q_1^{div} - Q_0$ element

3.1 Position of the problem

For the volumic unknowns, we introduce a regular mesh $\mathcal{T}_h$ of the rectangular domain C composed of square elements of length h. In [4], we introduced for the problem without obstacle new mixed finite elements, the so-called $Q_{k+1}^{div} - Q_k$ elements, inspired by Nédélec's second family [20]. These elements are compatible with mass lumping, and therefore allow for constructing an explicit scheme in time. A non standard convergence analysis of these $Q_{k+1}^{div} - Q_k$ elements was carried out in [4]. Naturally, our first choice for the problem with an obstacle was naturally the lowest order element $Q_1^{div} - Q_0$ for the velocity and the pressure fields,

$$\left\{ \begin{array}{l} \underline{X_h} = \{\mathbf{w}_h \in \underline{X} \,/\, \forall K \in \mathcal{T}_h,\ \mathbf{w}_h|_K \in Q_1 \times Q_1\}, \\ M_h = M_h^0 \quad \text{with} \quad M_h^0 = \{q_h \in M \,/\, \forall K \in \mathcal{T}_h,\ q_h|_K \in Q_0\}. \end{array} \right. \tag{9}$$

For more details on this element we refer to [4]. Notice that the velocity approximation space $\underline{X_h}$ contains the lower order Raviart Thomas element,

$$\underline{X_h}^{RT} = \{\mathbf{w}_h \in \underline{X} \,/\, \forall K \in \mathcal{T}_h,\ \mathbf{w}_h|_K \in P_{10} \times P_{01}\}.$$

For the approximation of the Lagrange multiplier, we introduce a mesh of Γ composed of N curvilinear segments S_j of length H_j, and we set $H = \sup_j H_j$. We assume that this mesh is uniformly regular,

$$\exists \nu,\ 0 < \nu \leq 1,\ \text{such that}\ : \forall j,\ 1 \leq j \leq N,\ H_j \geq \nu H. \tag{10}$$

We then choose the space of continuous linear piecewise functions:

$$\mathcal{G}_H = \left\{ \nu_H \in \mathcal{G} \,/\, \forall S_j,\ j = 1, \ldots, N,\ \nu_H\big|_{S_j} \in P_1 \right\}. \tag{11}$$

The spaces $(\underline{X_h}, M_h^0, \mathcal{G}_H)$ clearly satisfy the approximation properties (7). This choice which seemed to us natural, since the convergence was proven without obstacle, is the one that was used in [5] for the more complex elastodynamic case. However we have not been able to prove the convergence of the fictitious domain method with these spaces.

The convergence analysis of the fictitious domain method applied to other problems [1, 12, 18] shows that convergence holds if a compatibility condition between the step sizes of the two meshes is satisfied,

$$H \geq \alpha h. \tag{12}$$

We will show in what follows some numerical illustrations which seem to indicate that for some special configurations of obstacles, the method does not converge.

3.2 Numerical illustrations

The computational domain is the square $[0, 10]mm \times [0, 10]mm$ composed by a homogeneous isotropic material with $\rho = 1000$Kgr/m^3 and $\mathbf{A} = I \times 10^9$Pa. It is excited by an initial condition on the pressure centered on $(x_c, z_c) = (5, 5)$mm,

$$p((x, z), t = 0) \quad = \quad 0.1\ F\left(\frac{r}{r_0}\right),$$

where $F(r)$ is supported in $[0, 1]$ and given by (for $r \in [0, 1]$)

$$F(r) \quad = \quad A_0 - A_1 \cos(2\pi r) + A_2 \cos(3\pi r) - A_3 \cos(6\pi r),$$

with $\mathbf{r} = (x - x_c, z - z_c)^t$, $r = \|\mathbf{r}\|$, $r_0 = 1$mm and

$$A_0 = 0.35875, \quad A_1 = 0.48829, \quad A_2 = 0.14128, \quad A_3 = 0.01168.$$

We consider a uniform mesh of squares using a discretization step $h = 0.025$mm. The time discretization is done using a leap frog scheme with the time step Δt chosen in such a way that the ratio $\Delta t/h$ is equal to the maximal value that ensures the stability. Perfectly matched layers are used to simulate a non bounded domain.

Horizontal obstacle. In the first experiment we consider a plane horizontal crack

$$(x, z) \quad = \quad (5 + 2\sqrt{2}(2t - 1), 5 - 2\sqrt{2})\text{mm}, \qquad t \in [0, 1], \tag{13}$$

that we discretize using a uniform mesh of step $H = Rh$. The method converges and we obtain good results for reasonable values for the parameter R (in the interval $[0.75, 3]$). In the first column of figure 2 we show the results for $R = 1.2$. At the beginning, the wave is totally

reflected by the boundary. When the wave front reach the tips of the crack, two scattered waves are created.

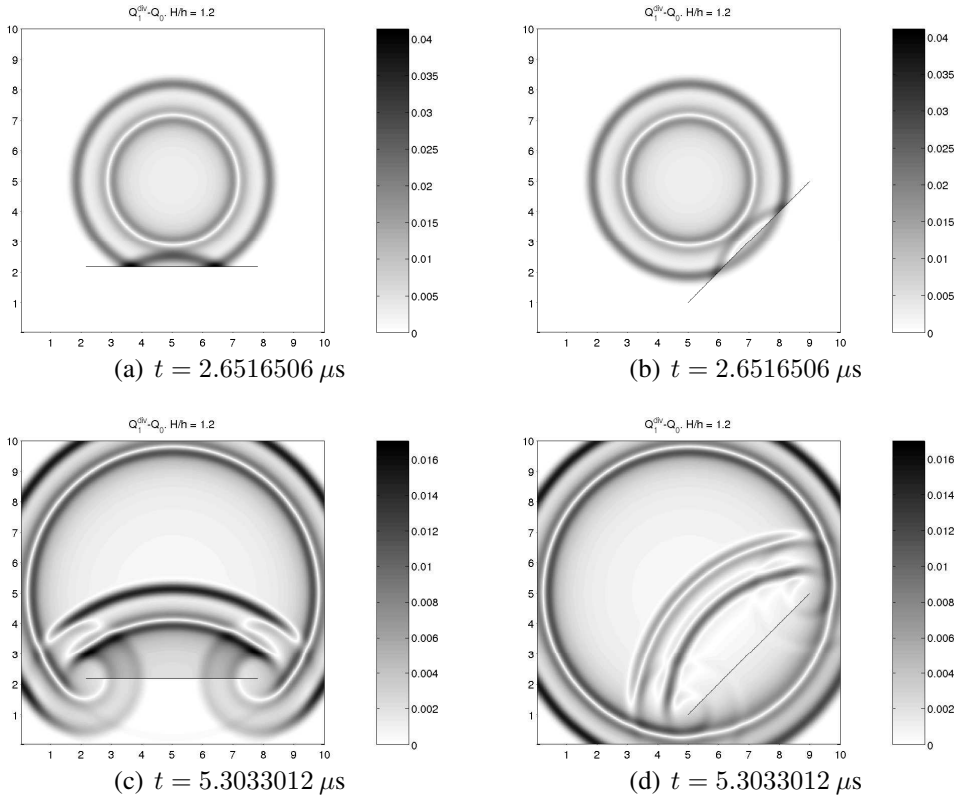

(a) $t = 2.6516506\ \mu$s (b) $t = 2.6516506\ \mu$s

(c) $t = 5.3033012\ \mu$s (d) $t = 5.3033012\ \mu$s

Figure 2: $Q_1^{div} - Q_0$. Isotropic medium. $H/h = 1.2$

Diagonal obstacle. In the second experiment we treat a plane diagonal defect given by

$$(x, z) \quad = \quad (5 + 4t, 1 + 4t)\text{mm}, \qquad t \in [0, 1], \tag{14}$$

that is, the same obstacle considered in the previous paragraph rotated by $\pi/4$ radians with respect to (x_c, z_c), the center of the initial condition. As the medium is isotropic, the solution of the continuous problem is also a rotation of the solution with the horizontal crack.

We discretize the Lagrange multiplier using again a uniform mesh of step $H = Rh$ with several values for the parameter R. However, this time, the approximated solution does not seem to converge towards the physical solution (see for instance the second column of the figure 2 for $R = 1.2$). The incident wave is not completely reflected but also transmitted through the interface.

4 The modified element $Q_1^{div} - P_1^{disc}$

4.1 Presentation of the modified element

We propose to modify the space M_h in such a way that

$$\text{div}\left(\underline{X_h}\right) \subset M_h, \tag{15}$$

which could simplify the analysis. In particular, we discretize the pressure in the space

$$M_h = M_h^1 \quad \text{with} \quad M_h^1 = \{q_h \in M \,/\, \forall K \in \mathcal{T}_h,\ q_h|_K \in P_1(K)\}\,. \tag{16}$$

Since $M_h^0 \subset M_h^1$ we have obviously

$$\inf_{q_h \in M_h} \|p - q_h\|_\rho \leq \inf_{q_h^0 \in M_h^0} \left\|p - q_h^0\right\|_\rho,$$

so that the approximation properties (7) are still satisfied.

4.2 Some numerical illustrations using the modified element

Let us now show some numerical illustrations of the behavior of the fictitious domain method with the new finite element space. The numerical experiments that we have considered are the same as in section 3.2 and will allow us to compare both finite elements.

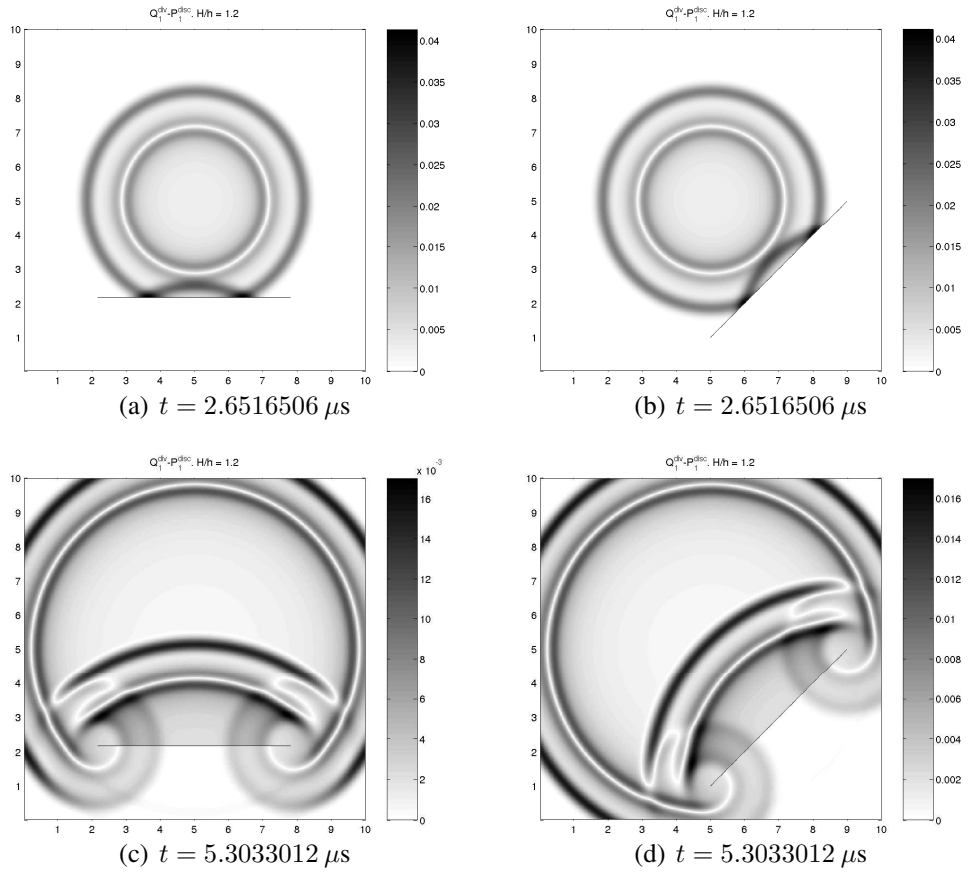

(a) $t = 2.6516506\ \mu$s (b) $t = 2.6516506\ \mu$s

(c) $t = 5.3033012\ \mu$s (d) $t = 5.3033012\ \mu$s

Figure 3: $Q_1^{div} - P_1^{disc}$. Isotropic medium. $H/h = 1.2$

Horizontal obstacle Once again we discretize the horizontal crack defined by (13) using a uniform mesh of step $H = Rh$. The results obtained with the new mixed finite element $Q_1^{div} - P_1^{disc}$ are similar to those given by the $Q_1^{div} - Q_0$ element. The method converges for reasonable values of the parameter R (in the interval $[0.75, 3]$). In the first column of the figure 3 we can see the results for $R = 1.2$.

Diagonal obstacle We now consider the diagonal crack defined by the expression (14). We recall that the continuous problem is a rotation of $\pi/4$ radians with respect to the point $(x_c, z_c) = (5, 5)$. The Lagrange multiplier is again discretized using an uniform mesh of step $H = Rh$. Contrary to the results obtained with the element $Q_1^{div} - Q_0$, the ones given by the modified element $Q_1^{div} - P_1^{disc}$ converge towards the physical solution when choosing reasonable values for the ratio H/h. As we show in the second column of figure 3, this time the incident wave is almost completely reflected by the obstacle. The scattered waves created by the tips of the crack are well approximated.

4.3 Damping of the spurious modes

Using a dispersion analysis we have shown [7] that the modified element gives rise to some spurious modes. In this section we propose a way to damp the amplitude of these modes (without damping the "physical part"), so that they do not perturb too much the approximate solution.

The modified space M_h^1 can be decomposed as

$$M_h = M_h^0 \oplus M_h^r, \tag{17}$$

where M_h^0 is the space of piecewise constants and M_h^r is its orthogonal complement (for the L^2 scalar product). The space M_h^r is composed of P_1 discontinuous functions with vanishing mean value per element.

From the dispersion analysis, we observe that the main components of the spurious modes (the O(1) part) belong to M_h^r. In order to damp this main part, we introduce the L^2 orthogonal projection on M_h^r, that we denote by $P_{M_h^r}$, defined for any $p \in M_h$ as,

$$P_{M_h^r}(p) \in M_h^r \quad \text{and} \quad (P_{M_h^r}(p), q_h) = (p, q_h), \quad \forall q_h \in M_h^r.$$

The approximate problem with damping consists in finding $(p_h, \mathbf{v}_h) \in M_h \times \underline{X_h}$ such that

$$\begin{cases} \dfrac{d}{dt} a(\mathbf{v}_h, \mathbf{w}_h) + b(\mathbf{w}_h, p_h) - < \mathbf{w}_h \cdot n, \lambda_H >_\Gamma = 0, \quad \forall \mathbf{w}_h \in \underline{X_h}, \\ \dfrac{d}{dt}(p_h, q_h)_\rho + (P_{M_h^r}(p_h), q_h)_\beta - b(\mathbf{v}_h, q_h) = (f, q_h), \quad \forall q_h \in M_h, \\ < \mathbf{v}_h \cdot n, \mu_H >_\Gamma = 0, \quad \forall \mu_H \in \mathcal{G}_H. \end{cases} \tag{18}$$

In this system β represents a damping parameter, which is chosen as a positive constant in the applications. The case $\beta = 0$ gives back the non-damped problem, while a strictly positive β corresponds to a dissipative problem. From the numerical point of view, it remains to define a procedure in order to choose this parameter in an appropriate way.

Remark 2 *The convergence analysis for (18) was carried out in [7] and error estimates were obtained.*

5 Numerical error estimates

In this section we are interested in estimating numerically the order of convergence of the method. To do so, we consider solving the wave equation on a disk $\Omega \subset I\!R^2$ with homogeneous Neumann boundary conditions on its boundary $\Gamma = \partial\Omega$. The geometry of the problem is presented in Figure 4.

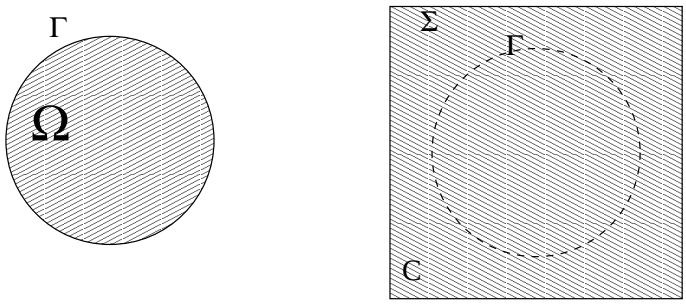

Figure 4: The geometry of the problem. On the left the initial domain of propagation Ω and on the right the extended domain, C, introduced by the fictitious domain formulation of the problem.

To compute the solution we extend the unknowns in the domain of simple geometry C (see Figure 4) and use the fictitious domain formulation (5) with a zero force term $f = 0$ and the initial conditions given in section 3.2. The center of the initial condition, $(x_c, z_c) = (5, 5)$mm, coincides with the center of the disk Ω whose radius is $R = 4mm$. The physical properties of the material and size of the computational domain are the same as in section 3.2. In practice to truncate the extended domain C, we surround the computational domain by a perfectly matched absorbing layer model (PML, [8, 10]).

We remark that the solution of this problem is rotationally invariant because of the symmetry in the geometry and the initial conditions. We use this symmetry in order to compute a reference solution by solving an one dimensional problem. More precisely, when expressed in cylindrical coordinates, it is easy to see that the solution of the two dimensional problem, (Ω being $[0, R] \times [0, 2\pi]$, and where $\varrho = 1000$Kgr/m^3 and $a = 10^9$Pa),

$$\left|\begin{array}{ll} a\dfrac{\partial v_r}{\partial t} - \dfrac{\partial p}{\partial r} = 0, & \text{in } [0, R] \times [0, 2\pi], \\ a\dfrac{\partial v_\theta}{\partial t} - \dfrac{\partial p}{\partial \theta} = 0, & \text{in } [0, R] \times [0, 2\pi], \\ \varrho\dfrac{\partial p}{\partial t} - \dfrac{\partial v_r}{\partial r} - \dfrac{1}{r}v_r = 0, & \text{in } [0, R] \times [0, 2\pi], \\ v_r = 0, & \text{on } [r = R] \times [0, 2\pi], \end{array}\right.$$

with initial conditions,

$$p_0(r, \theta) = 0.1F(r/r_0),\ v_r = v_\theta = 0,$$

depends only on r, i.e., $v_r(r, \theta) = v_r(r), v_\theta = 0,\ p(r, \theta) = p(r)$. Thus, it can be deduced by solving the following one-dimensional problem,

$$\left|\begin{array}{ll} a\dfrac{\partial v_r}{\partial t} - \dfrac{\partial p}{\partial r} = 0, & \text{in } [0, R], \\ \varrho\dfrac{\partial p}{\partial t} - \dfrac{\partial v_r}{\partial r} - \dfrac{1}{r}v_r = 0, & \text{in } [0, R], \\ v_r = 0, & \text{for } r = 0 \text{ and } r = R, \end{array}\right. \tag{19}$$

with initial conditions,

$$p(r, t = 0) = 0.1F(r/r_0),\ v_r(t = 0, r) = 0.$$

To solve numerically the one dimensional problem (19), we use piecewise constant functions for the discretization of p_r and continuous piecewise linear functions for v_r. For the time discretization a second order leap frog scheme is employed.

In figure 5 we display the results of the numerical convergence analysis. The reference solution in 1D, is obtained on a fine grid with a space discretization step $h_{1d} = 1/160$mm. The two dimensional problem is solved with four different discretizations using $h_x = h_z = h = 1/10, 1/20, 1/40$ and $1/80$mm. For each discretization we compute the difference between the obtained solution and the reference one. In figure 5 we display the logarithm of the error as a function of the logarithm of the discretization step. The rate of convergence is deduced from the slope s of the line. We can remark that the results obtained numerically are slightly better than our theoretical predictions. Note however, that the estimate obtained on the $L^\infty([0,T], H(\mathrm{div}))$ norm of $\mathbf{v}$ is $h^{0.48}$ which indicates that the theoretical estimations are optimal (cf. [7]).

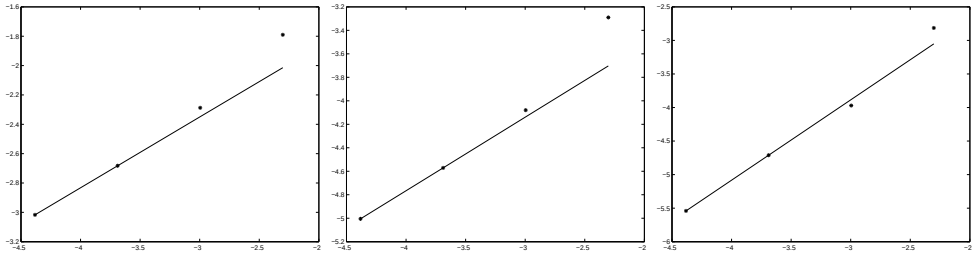

(a) $\sup_{t\leq T} \|\mathbf{v} - \mathbf{v}_h\|_{\underline{X}}$, $s = 0.48$. (b) $\sup_{t\leq T} \|p - p_h\|_M$, $s = 0.63$. (c) $\sup_{t\leq T} \|\lambda - \lambda_h\|_{\mathcal{G}}$, $s = 1.2$.

Figure 5: Numerical error on $\mathbf{v}$, p and λ versus the discretization step.

In figure 6 we display the same results but with the norm of the error now computed in $\widetilde{C} = C/B_b(\Gamma)$, i.e., the domain C restricted from $B_b(\Gamma)$, defined by

$$B_b(\Gamma) = \left\{ \mathbf{x} \in C \text{ s.t. } \min_{\mathbf{y}\in\Gamma} |\mathbf{x} - \mathbf{y}| \leq b \right\}. \tag{20}$$

We observe that the convergence rate of the method is higher, actually one approximately recovers the order of convergence of the method without obstacle, here $O(h)$. Furthermore, we remarked numerically that $b = h$ is the critical value, i.e., the convergence rate does not change for bigger values of b and it decreases for $b < h$. This agrees with our intuition in the sense that the elements that we need to remove are the ones in which the solution has less regularity (see remark 1), i.e., the elements that have non-zero intersection with the boundary Γ. Finally, notice that the rate of convergence on λ (approximately 1) is higher than expected (1/2). We conjecture that this is due to the closed boundary of the object and that this rate would be lower for a crack (see remark 1).

6 Extension to the elastodynamic case

We consider in this section the problem of elastic wave scattering by a crack. The generalization of the fictitious domain method to this case was presented in [5]. For the space discretization of the volume unknowns, which are in this case the stress tensor and the velocity field, an original finite element method was proposed and analyzed in [6]. The lower order elements of this family coupled with piecewise linear continuous elements for the surface unknown were used in [5]. This choice corresponds to the vectorial analogue of the $Q_1^{div} \times Q_0$

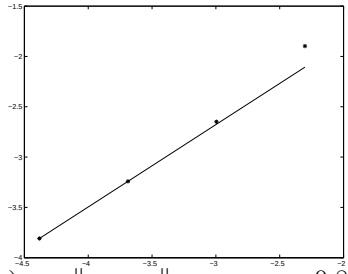

(a) $\sup_{t\leq T} \|\mathbf{v}-\mathbf{v}_h\|_{\underline{H_{div}}(\widetilde{C})}$. $s=0.82$.

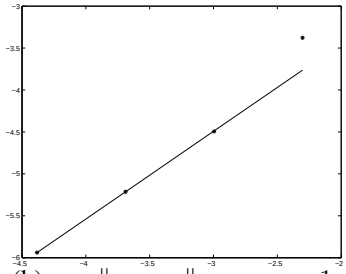

(b) $\sup_{t\leq T} \|p-p_h\|_{L^2(\widetilde{C})}$. $s=1$.

Figure 6: Numerical error on $\mathbf{v}$, p and λ versus the discretization step. Here we compute the norm of the error in the domain $\widetilde{C}$ which is C restricted from $B_b(\Gamma)$, i.e., Γ and its vicinity (20).

element coupled with P_1 continuous elements on the crack that was discussed in section 3. Also here, the same questions and difficulties arise. Namely, from the theoretical point of view, the convergence of the method was not proved and numerical examples indicate that for some crack geometries the method does not converge. The solution we propose is to use instead the modified $Q_1^{div} \times P_1^{disc}$ element. As for the case without crack, the theoretical convergence of the method is not a straightforward generalization of the scalar case. Although we were not able to prove the convergence of the method theoretically we will show numerical results that indicate that the method converges.

We briefly present in the following the continuous elastodynamic problem, the finite elements used for the space discretization and the numerical results obtained in this case.

6.1 The continuous problem

Consider the geometry given in Fig. 1 and assume now that the material filling Ω is an elastic solid. In this case, and under the assumption of small deformations, wave propagation is governed by the linear elastic wave equations,

$$\left\{\begin{array}{l} \text{Find } (\boldsymbol{\sigma},\mathbf{v}) : (x,t)\in\Omega\times[0,T]\mapsto(\boldsymbol{\sigma}(x,t),\mathbf{v}(x,t))\in\mathbb{R}^4\times\mathbb{R}^2 \text{ satisfying,} \\ \rho\dfrac{\partial \mathbf{v}}{\partial t} - \text{div}\,\boldsymbol{\sigma} = \mathbf{f}, \quad \text{in } \Omega, \quad (a) \\ \mathbf{A}\dfrac{\partial \boldsymbol{\sigma}}{\partial t} - \boldsymbol{\varepsilon}(\mathbf{v}) = 0, \quad \text{in } \Omega, \quad (b) \\ \boldsymbol{\sigma}\mathbf{n} = 0, \quad \text{on } \Gamma, \quad (c) \\ \mathbf{v} = 0, \quad \text{on } \Sigma, \quad (d) \end{array}\right. \tag{21}$$

together with the initial conditions,

$$\left\{\begin{array}{l} \mathbf{v}(t=0) = \mathbf{v}_0, \\ \boldsymbol{\sigma}(t=0) = \boldsymbol{\sigma}_0. \end{array}\right. \tag{22}$$

In (21), $\mathbf{v}$ is the velocity field and $\boldsymbol{\sigma}$ the stress tensor. This formulation is preferred to the classical displacement formulation because the boundary condition on the crack is natural (of Neumann type) for the displacement while it becomes essential on $\boldsymbol{\sigma}$ and the fictitious domain approach can then be followed. Note that the couple $(\boldsymbol{\sigma},\mathbf{v})$ plays the same role here as the

couple $(\mathbf{v}, p)$ in the scalar case. The matrix $\mathbf{A}$ becomes now a fourth-order symmetric definite positive tensor. The fictitious domain formulation is

$$\left\{\begin{array}{lllllll} \text{Find } (\boldsymbol{\sigma}(t), \mathbf{v}(t), \boldsymbol{\lambda}(t)) \in \underline{\underline{X}}^{sym} \times \underline{M} \times \underline{\mathcal{G}} \text{ satisfying,} & & & & & & \\ \dfrac{\mathrm{d}}{\mathrm{d}t} a(\boldsymbol{\sigma}, \boldsymbol{\tau}) & + & b(\boldsymbol{\tau}, \mathbf{v}) & - & < \boldsymbol{\tau}\mathbf{n}, \boldsymbol{\lambda} >_\Gamma & = & 0, \qquad \forall \boldsymbol{\tau} \in \underline{\underline{X}}^{sym}, \\ \dfrac{\mathrm{d}}{\mathrm{d}t} (\mathbf{v}, \mathbf{w})_\rho & - & b(\boldsymbol{\sigma}, \mathbf{w}) & & & = & (\mathbf{f}, \mathbf{w}), \qquad \forall \mathbf{w} \in \underline{M}, \\ & & & & < \boldsymbol{\sigma}\mathbf{n}, \boldsymbol{\mu} >_\Gamma & = & 0, \qquad \forall \boldsymbol{\mu} \in \underline{\mathcal{G}}, \\ (\boldsymbol{\sigma}, \mathbf{v})_{/t=0} & & & & & = & (\boldsymbol{\sigma}_0, \mathbf{v}_0), \end{array}\right. \tag{23}$$

where the bilinear forms are defined by (6) with the obvious changes. The functional spaces are

$$\underline{\underline{X}}(= \underline{\underline{X}}(C)) = \underline{X} \times \underline{X}, \quad \underline{M} = M \times M, \quad \underline{\mathcal{G}} = \mathcal{G} \times \mathcal{G},$$

and the stress tensor belongs to the subspace of symmetric tensors in $\underline{\underline{X}}$,

$$\underline{\underline{X}}^{sym} = \left\{ \sigma \in \underline{\underline{X}} \,/\, \mathrm{as}(\sigma) = 0 \right\},$$

with $\mathrm{as}(\sigma)$ defined in 2D by,

$$\mathrm{as}(\sigma) = \sigma_{12} - \sigma_{21}.$$

6.2 The approximate problem

The semi-discrete formulation For the approximation in space of this problem, we introduce finite dimensional spaces $\underline{\underline{X_h}}^{sym} \subset \underline{\underline{X}}^{sym}$, $\underline{M_h} \subset \underline{M}$ and $\underline{\mathcal{G}_H} \subset \underline{\mathcal{G}}$ satisfying the usual approximation properties,

$$\left|\begin{array}{lll} \inf\limits_{h\geq 0} \inf\limits_{\boldsymbol{\tau}_h \in \underline{\underline{X_h}}^{sym}} \|\boldsymbol{\tau} - \boldsymbol{\tau}_h\|_{\underline{\underline{X}}} & = & 0, \quad \forall \boldsymbol{\tau} \in \underline{\underline{X}}^{sym}, \\ \inf\limits_{h\geq 0} \inf\limits_{\mathbf{v}_h \in \underline{M_h}} \|\mathbf{v} - \mathbf{v}_h\|_{\underline{M}} & = & 0, \quad \forall \mathbf{v} \in \underline{M}, \\ \inf\limits_{H\geq 0} \inf\limits_{\boldsymbol{\mu}_H \in \underline{\mathcal{G}_H}} \|\boldsymbol{\mu} - \boldsymbol{\mu}_H\|_{\underline{\mathcal{G}}} & = & 0, \quad \forall \boldsymbol{\mu} \in \underline{\mathcal{G}}. \end{array}\right. \tag{24}$$

The semi-discrete problem is then,

$$\left\{\begin{array}{lllllll} \text{Find } (\boldsymbol{\sigma}_h(t), \mathbf{v}_h(t), \boldsymbol{\lambda}_H(t)) \in \underline{\underline{X_h}}^{sym} \times \underline{M_h} \times \underline{\mathcal{G}_H} \text{ such that,} & & & & & & \\ \dfrac{\mathrm{d}}{\mathrm{d}t} a(\boldsymbol{\sigma}_h, \boldsymbol{\tau}_h) & + & b(\boldsymbol{\tau}_h, \mathbf{v}_h) & - & < \boldsymbol{\tau}_h \cdot \mathbf{n}, \boldsymbol{\lambda}_H >_\Gamma & = & 0, \qquad \forall \boldsymbol{\tau}_h \in \underline{\underline{X_h}}^{sym}, \\ \dfrac{\mathrm{d}}{\mathrm{d}t} (\mathbf{v}_h, \mathbf{w}_h)_\rho & - & b(\boldsymbol{\sigma}_h, \mathbf{w}_h) & & & = & (f, \mathbf{w}_h), \quad \forall \mathbf{w}_h \in \underline{M_h}, \\ & & & & < \boldsymbol{\sigma}_h \cdot \mathbf{n}, \boldsymbol{\mu}_H >_\Gamma & = & 0, \qquad \forall \boldsymbol{\mu}_H \in \underline{\mathcal{G}_H}, \\ \boldsymbol{\sigma}_h(t=0) & = & \boldsymbol{\sigma}_{h,0}, & & & & \\ \mathbf{v}_h(t=0) & = & \mathbf{v}_{h,0}, & & & & \end{array}\right. \tag{25}$$

and where $(\boldsymbol{\sigma}_{h,0}, p_{h,0}) \in \underline{\underline{X_h}}^{sym} \times \underline{M_h}$ is an approximation of the exact initial condition.

The two families of mixed finite elements. Following the same ideas as for the scalar problem, an original finite element for the elastodynamic system which is compatible with mass lumping was introduced in [6]. The difference with the $Q_{k+1}^{div} - Q_k$ elements is due to the symmetry of the stress tensor. Namely the lowest order element in this case is,

$$\begin{cases} \underline{\underline{X_h}} = \left\{ \boldsymbol{\tau}_h \in \underline{\underline{X}} \,/\, \forall K \in \mathcal{T}_h,\ \boldsymbol{\tau}_h|_K \in (Q_1 \times Q_1)^2 \right\}, \\ \underline{\underline{X_h}}^{sym} = \left\{ \boldsymbol{\tau}_h \in \underline{\underline{X_h}} \,/\, \mathrm{as}(\boldsymbol{\tau}_h) = 0 \right\}, \qquad \underline{M_h} = \underline{M_h}^0 = (M_h^0)^2, \end{cases} \tag{26}$$

M_h^0 being defined as for the scalar case. Another characterization $\underline{\underline{X_h}}^{sym}$ is

$$\begin{aligned} \underline{\underline{X_h}}^{sym} = \ & \{\sigma_{12} \in H^1(\Omega)/\sigma_{12}\,|_K \in Q_1,\ \forall K \in \mathcal{T}_h \ \text{ and} \\ & (\sigma_{11}, \sigma_{22}) \in H(\mathrm{div}, \Omega)/(\sigma_{11}, \sigma_{22})\,|_K \in (Q_1)^2,\ \forall K \in \mathcal{T}_h \} . \end{aligned} \tag{27}$$

We obviously do not have $\underline{\underline{X_h}}^{sym} = \underline{X_h} \times \underline{X_h}$. This implies in particular that the approximation space $\underline{\underline{X_h}}^{sym}$ does not contain the lowest order Raviart Thomas element. Convergence results and error estimates for the problem without Lagrange multiplier were obtained in [6].

We recall here the approximation properties for the space $\underline{\underline{X_h}}^{sym}$. Let $\tau \in \underline{\underline{X}}^{sym}$ with $(\tau_{11}, \tau_{22}) \in H^{1,0} \times H^{0,1}$ (cf. [6] for more details), and $\tau_{12} = \tau_{21} \in H^1$ then

$$\lim_{h \to 0} \inf_{\boldsymbol{\tau}_h \underline{\underline{X_h}}^{sym}} \|\boldsymbol{\tau} - \boldsymbol{\tau}_h\|_{\underline{\underline{X}}} = 0.$$

Moreover, if $(\tau_{11}, \tau_{22}) \in H^{2,1} \times H^{1,2}$ and $\tau_{12} \in H^2$ then

$$\inf_{\boldsymbol{\tau}_h \in \underline{\underline{X_h}}^{sym}} \|\boldsymbol{\tau} - \boldsymbol{\tau}_h\|_{\underline{\underline{X}}} \leq Ch(|\tau_{11}|_{H^{2,1}} + |\tau_{22}|_{H^{1,2}} + |\tau_{12}|_{H^2}). \tag{28}$$

The approximation of the Lagrange multiplier is done in the space $\underline{\mathcal{G}_H} = (\mathcal{G}_h)^2$, $\mathcal{G}_h$ being defined by (11). The spaces $(\underline{M_h}^0, \underline{\mathcal{G}_H})$ satisfy the usual approximation properties (7).

The choice of the above approximation spaces seemed once again reasonable. However, as for the scalar case no theoretical convergence results were obtained for the fictitious domain formulation. Moreover, numerical examples indicate that for some crack geometries the method does not converge. To face this drawback, the same approach as for the scalar case was followed. The modified element consists in this case to discretize the velocity in $\underline{M_h}^1 = (M_h^1)^2$. From the numerical point of view this choice introduces spurious modes in the velocity whose amplitude is more important than in the scalar case. The selective damping of the spurious modes is achieved using the same tools as in section 4.3. Namely, the second equation of (25) is replaced by

$$\frac{\mathrm{d}}{\mathrm{d}t}(\mathbf{v}_h, \mathbf{w}_h)_\rho + (P_{\underline{M_h}^r}(\mathbf{v}_h), \mathbf{w}_h)_\beta - b(\boldsymbol{\sigma}_h, \mathbf{w}_h) = (f, \mathbf{w}_h), \quad \forall \mathbf{w}_h \in \underline{M_h},$$

where $\underline{M_h}^r = (M_h^r)^2$ and β is the damping parameter.

Convergence issues. From the numerical point of view we observe that the method converges under a compatibility condition of the form (12) between the two discretization meshes. From the theoretical point of view the convergence proof in this case is not a straightforward generalization of the acoustic case [7]. The main difficulty comes from the non standard regularity required to obtain the approximation properties for $\underline{\underline{X_h}}^{sym}$ (see (28)). Indeed, the maximal regularity (in space) of the stress tensor in the case of a domain with a crack is $\boldsymbol{\sigma} \in (H^{\frac{1}{2}-\varepsilon}(\mathrm{div}, C))^2$, and $\boldsymbol{\sigma}$ is symmetric. This regularity is not sufficient to obtain (28) and thus we cannot conclude.

7 Numerical illustrations

We present in what follows some numerical results that illustrate the difficulties related with the convergence of the method that we discussed in the previous section. The computational domain is again the square $[0, 10] \times [0, 10]\ mm^2$ composed by an homogeneous isotropic material with density and Lame coefficients given by

$$\rho \;=\; 1000\ \text{Kgr/m}^3, \quad \lambda \;=\; 3.45 \times 10^9\ \text{Pa}, \quad \mu \;=\; 2.04 \times 10^9\ \text{Pa}. \tag{29}$$

We introduce an initial condition on the velocity field centered on $(x_c, z_c) = (5, 5)$mm,

$$\mathbf{v}((x, z), t = 0) \;=\; 0.1\ F\left(\frac{r}{r_0}\right)\frac{\mathbf{r}}{r},$$

where $F(\cdot)$, $\mathbf{r}$ and r have been defined in section 3.2 and $r_0 = 1.5$mm. We consider the diagonal crack parameterized by (14) on which we impose a free surface boundary condition. We use a mesh composed by squares with a discretization step $h = 0.025$mm. For the time discretization we use again a leap frog scheme with a time step Δt such that the ratio $\Delta t/h$ is equal to the maximal value that guarantees the stability. The crack is also discretized using a regular mesh with $H = 1.2h$. Perfectly matched layers are used to bound the computational domain.

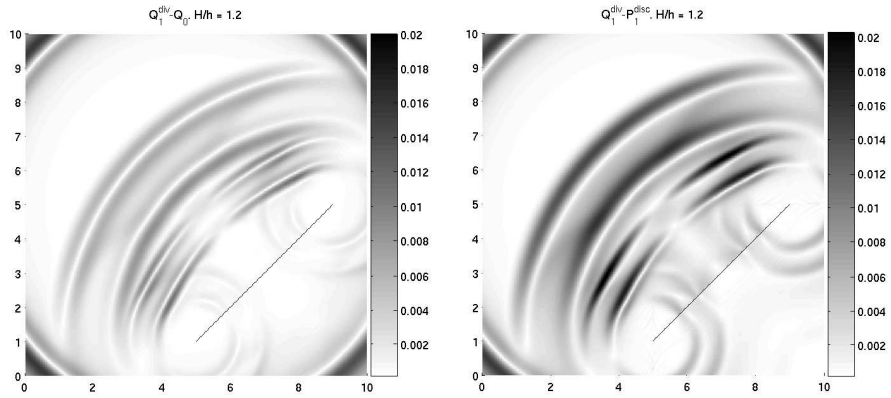

(a) $Q_1^{div} \times Q_0$ (b) $Q_1^{div} \times P_1^{disc}$

Figure 7: Modulus of the velocity field at $t = 2.5965\ \mu$s.

Results with the $Q_1^{div} \times Q_0$ element. When we use the original finite element, the incident wave (which is here a pressure wave) is not completely reflected by the obstacle but also transmitted as it can be clearly seen in figure 7-(a). Similar results are also obtained when using other ratios between H and h and when refining the meshes. This indicates the lack of convergence as for the scalar case.

Results with the $Q_1^{div} \times P_1^{disc}$ element. The solution obtained with the new finite element seems to converge towards the solution of the continuous problem. The incident wave is completely reflected by the obstacle and the scattered waves generated by the extremities of the crack are well approximated (see figure 7-(b)). As for the scalar case, the enrichment of $\underline{M_h}$ introduces spurious modes in the solution. Although the amplitude of these non-physical waves

goes to zero with the size of the discretization step, it is still significant for usual choices of the discretization parameters, typically corresponding to 20 points per wavelength. These spurious modes are for example visible in the results presented in figure 8-(a) where we have amplified by a factor eight the results of figure 7-(b).

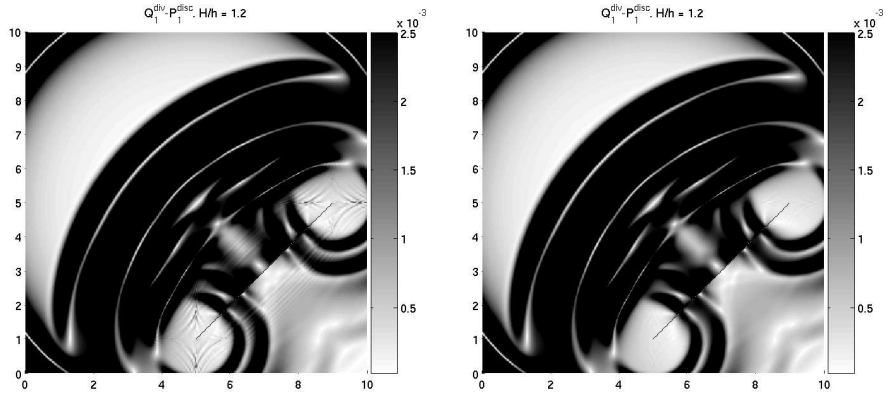

(a) $Q_1^{div} \times P_1^{disc},\ \beta = 0$ (b) $Q_1^{div} \times P_1^{disc},\ \beta = 5\varrho 10^6$

Figure 8: Modulus of the velocity field $\times 8$ at $t = 2.5965\ \mu$s.

Influence of the damping parameter on the solution. To illustrate the effect of the damping parameter β on the solution we present in figure 9 results obtained for different values of β. We have made the following observations: when we do not use any damping, the solution is polluted by spurious modes. On the other hand, the amplitude of the transmitted (non-physical) waves through the crack increases as the value of the damping β increases. This is expected because the limit case $\beta \to +\infty$ corresponds to seeking the velocity in Q_0 and we know that in this case, the method does not converge. There is thus an optimal value for the damping parameter β to be determined so as the spurious modes are damped while the transmitted non-physical wave remains small. In the next section we determine numerically the rate of convergence of the method for a particular geometry and we discuss a procedure for choosing the value of β.

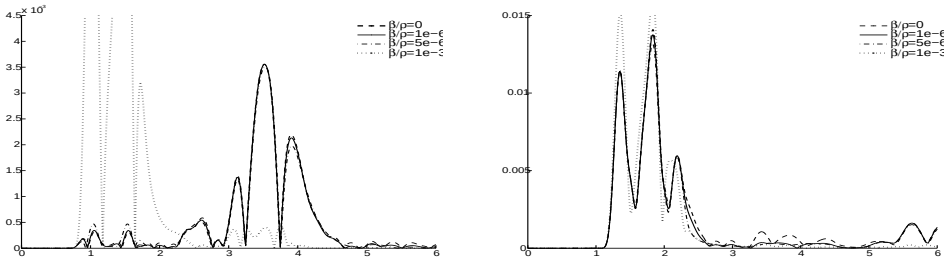

(a) $|v|((7.5, 2.5)\text{mm}, t)$ (b) $|v|((5.0, 0.5)\text{mm}, t)$

Figure 9: The modulus of the velocity $|\mathbf{v}|(\mathbf{x_i}, t),\ t \in [0, 6]\mu$s computed using the $Q_1^{div} \times P_1^{disc}$ element with $h = 0.025$mm and different values of the damping parameter β.

8 Numerical error estimates

In the same way as for the scalar case, we determine numerically the order of convergence of the fictitious domain method. To do so we consider the geometry in section 5 with $R = 4$ mm, no external forces and an initial condition on the velocity field given by

$$\mathbf{v}((x,z),t=0) \;=\; 0.1\,F\left(\frac{r}{r_0}\right)\frac{\mathbf{r}+\mathbf{r}^{\perp}}{r},$$

where $F(\cdot)$, $\mathbf{r}$ and r have been defined in section 3.2 and $r_0 = 1.5mm$. The domain of propagation is an isotropic medium with the density and Lame coefficients given by (29). The extended domain C introduced by the fictitious domain formulation is truncated using perfectly matched layers (PML, [8, 10]). We consider the final time equal to $T = 5\mu s$ when both, the pressure and shear waves have reached the boundary.

The fact of having a problem that is rotationally invariant allows us to compute a reference solution solving a 1D problem. More precisely, rewriting equations (21) in polar coordinates

$$\left|\begin{array}{rcll}
\rho\dfrac{\partial v_r}{\partial t} &=& \dfrac{\partial \sigma_{rr}}{\partial r} + \dfrac{1}{r}\dfrac{\partial \sigma_{r\theta}}{\partial \theta} + \dfrac{1}{r}(\sigma_{rr}-\sigma_{\theta\theta}), & \text{in } [0,R]\times[0,2\pi],\\
\rho\dfrac{\partial v_\theta}{\partial t} &=& \dfrac{\partial \sigma_{r\theta}}{\partial r} + \dfrac{1}{r}\dfrac{\partial \sigma_{\theta\theta}}{\partial \theta} + \dfrac{2}{r}\sigma_{r\theta}, & \text{in } [0,R]\times[0,2\pi],\\
\dfrac{\partial \sigma_{rr}}{\partial t} &=& (2\mu+\lambda)\dfrac{\partial v_r}{\partial r} + \lambda\dfrac{v_r}{r} + \lambda\dfrac{1}{r}\dfrac{\partial v_\theta}{\partial \theta}, & \text{in } [0,R]\times[0,2\pi],\\
\dfrac{\partial \sigma_{\theta\theta}}{\partial t} &=& (2\mu+\lambda)\left(\dfrac{1}{r}\dfrac{\partial v_\theta}{\partial \theta}+\dfrac{v_r}{r}\right) + \lambda\dfrac{\partial v_r}{\partial r}, & \text{in } [0,R]\times[0,2\pi],\\
\dfrac{\partial \sigma_{r\theta}}{\partial t} &=& \mu\left(\dfrac{1}{r}\dfrac{\partial v_r}{\partial \theta} + \dfrac{\partial v_\theta}{\partial r} - \dfrac{v_\theta}{r}\right), & \text{in } [0,R]\times[0,2\pi],\\
\sigma_{rr} = 0, \;\; \sigma_{r\theta} &=& 0, & \text{in } R\times[0,2\pi],
\end{array}\right. \tag{30}$$

with the initial conditions

$$v_s((r,\theta),t=0) \;=\; 0.1F(\frac{r}{r_0}), \quad s\in\{r,\theta\}, \tag{31}$$

we remark that the solution depends only on r and the former equations are equivalent to the two following decoupled one dimensional problems:

$$\left|\begin{array}{rcll}
\rho\dfrac{\partial v_r}{\partial t} &=& \dfrac{\partial \sigma_{rr}}{\partial r} + \dfrac{1}{r}(\sigma_{rr}-\sigma_{\theta\theta}), & \text{in } [0,R],\\
\dfrac{\partial \sigma_{rr}}{\partial t} &=& (2\mu+\lambda)\dfrac{\partial v_r}{\partial r} + \lambda\dfrac{v_r}{r}, & \text{in } [0,R],\\
\dfrac{\partial \sigma_{\theta\theta}}{\partial t} &=& (2\mu+\lambda)\dfrac{v_r}{r} + \lambda\dfrac{\partial v_r}{\partial r}, & \text{in } [0,R],\\
\sigma_{rr} &=& 0, & \text{in } R,
\end{array}\right. \tag{32}$$

$$\left|\begin{array}{rcll}
\rho\dfrac{\partial v_\theta}{\partial t} &=& \dfrac{\partial \sigma_{r\theta}}{\partial r} + \dfrac{2}{r}\sigma_{r\theta}, & \text{in } [0,R]\times[0,2\pi],\\
\dfrac{\partial \sigma_{r\theta}}{\partial t} &=& \mu\left(\dfrac{\partial v_\theta}{\partial r} - \dfrac{v_\theta}{r}\right), & \text{in } [0,R]\times[0,2\pi],\\
\sigma_{r\theta} &=& 0, & \text{in } R\times[0,2\pi].
\end{array}\right. \tag{33}$$

We solve numerically those systems using piecewise constant functions for the discretization of the velocity field and continuous linear functions for the stress tensor. For the time discretization

we use a leap frog scheme. The reference solution is obtained using a very fine mesh ($h_{1d} \approx 1/800$). The two dimensional problem is solved using four different meshes with $h_z = h_z = 1/10, 1/20, 1/40$ and $1/80$. We use the larger time step Δt authorized by the CFL condition. The mesh for the object is uniform and with a discretization step H such that $H/h \approx 1.2$ for each mesh. In all cases the damping parameter β is equal to zero. For each numerical experiment we compute the difference between the approximated solution and the reference solution. In figure 10 we display the logarithm of the error on the stress tensor, the velocity field and the Lagrange multiplier versus the logarithm of the discretization step. The rate of convergence is thus given by the slope of the lines. We observe that the order of convergence for σ in $L^\infty([0,T],(H(div,C))^2)$ norm and for $\mathbf{v}$ in $L^\infty([0,T],(L^2(C))^2)$ norm is near the value we could expect (i.e. $1/2$), while for λ in $L^\infty([0,T],(L^2(\Gamma))^2)$ is around 1 instead of $1/2$, which we beleive that it is due to the closed boundary geometry, as in the scalar case.

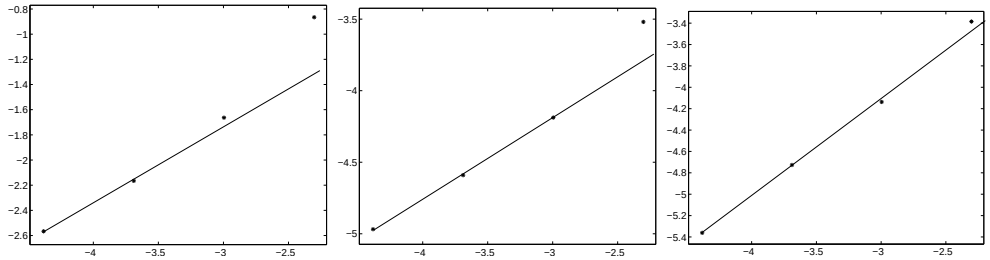

(a) $\sup_{t\leq T} \|\boldsymbol{\sigma} - \boldsymbol{\sigma}_h\|_{\underline{\underline{X}}}$, $s = 0.59$ (b) $\sup_{t\leq T} \|\mathbf{v} - \mathbf{v}_h\|_{\underline{M}}$, $s = 0.55$ (c) $\sup_{t\leq T} \|\boldsymbol{\lambda} - \boldsymbol{\lambda}_h\|_{\underline{\mathcal{G}}}$, $s = 0.92$

Figure 10: Numerical error on $\boldsymbol{\sigma}$, $\mathbf{v}$ and $\boldsymbol{\lambda}$ versus the discretization step.

In figure 11 we represent the logarithm of the errors on the stress tensor and the velocity field measured on $\widetilde{C} = C \setminus B_{0.15}(\Gamma)$. As for the scalar case we recover the order of convergence of the method without obstacle (i.e. O(h) here) when we remove a neighborhood of the object in which the solution is not very smooth.

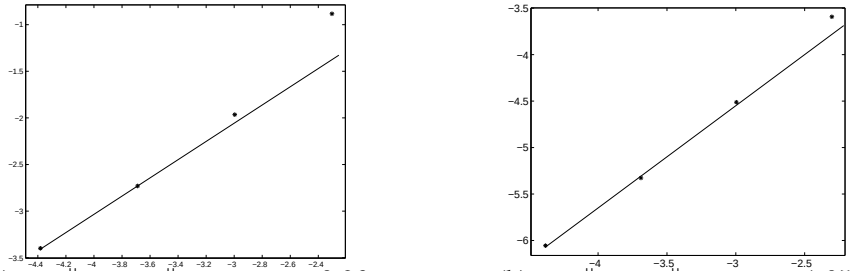

(a) $\sup_{t\leq T} \|\boldsymbol{\sigma} - \boldsymbol{\sigma}_h\|_{\underline{\underline{H_{div}}}(\widetilde{C})}$. $s = 0.96$. (b) $\sup_{t\leq T} \|\mathbf{v} - \mathbf{v}_h\|_{\underline{L^2}(\widetilde{C})}$. $s = 1.05$.

Figure 11: Numerical error $\boldsymbol{\sigma}$, $\mathbf{v}$ versus the discretization step. Here we compute the norm of the error on $\widetilde{C}$.

Finally we discuss the influence of the damping parameter β on the convergence results. In order to do so we repeat the experiment described above using the mesh with $h = 1/40$ mm for $\beta/\rho 10^{-6} = 0, 0.5, 2.5, 5, 7.5, 10, 12.5$ and 15 . We display on figure 12 the logarithm of the error on $\boldsymbol{\sigma}$, $\mathbf{v}$ and $\boldsymbol{\lambda}$ as a function of the value of $\beta/\rho 10^{-6}$. As we can see, better results are obtained for values of $\beta/\rho 10^{-6}$ between 2.5 and 5. We also observe that the error increases

when we choose β too large. The same experiments done for different materials show that the optimal range for β/ρ is independant of the material. It depends only on the number of points per wavelength in the discretization. It should be proportional to $1/\Delta t$: $\dfrac{\beta}{\rho} = \dfrac{\zeta}{\Delta t}$where ζ, an adimensional constant, determined by the previous experiment, should be chosen in the interval $[0.03, 0.06]$.

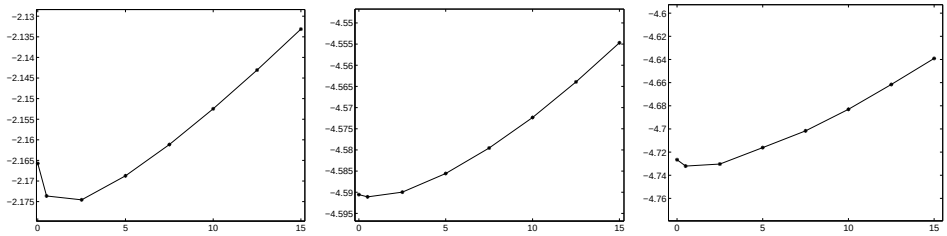

(a) $\sup_{t\leq T} \|\boldsymbol{\sigma} - \boldsymbol{\sigma}_h\|_{\underline{X}}$. (b) $\sup_{t\leq T} \|\mathbf{v} - \mathbf{v}_h\|_{\underline{M}}$. (c) $\sup_{t\leq T} \|\boldsymbol{\lambda} - \boldsymbol{\lambda}_h\|_{\underline{G}}$.

Figure 12: Numerical error on $\boldsymbol{\sigma}$, $\mathbf{v}$ and $\boldsymbol{\lambda}$ versus the damping parameter β/ρ.

Conclusion

We consider in this paper the application of the fictitious domain method for taking into account the Neumann boundary condition on the surface of a crack (or more generally an object) in the context of acoustic and elastic wave propagation. We first demonstrate with numerical examples that the method introduced in [5] does not converge for all crack geometries. We propose instead the use of a modified version of the mixed finite elements introduced in [4, 6]. Those elements consist in enriching the approximation space for the primal unknown. We carried out the theoretical and numerical convergence analysis of the method in the acoustic case (cf. [7]). In the elastic case, although not obtained theoretically, the convergence of the method is verified through extensive numerical simulations.

REFERENCES

[1] I. Babuska. The Finite Element Method with Lagrangian Multipliers. *Numer. Math.*, 20:179–192, 1973.

[2] E. Bécache, A. Chaigne, G. Derveaux, and P. Joly. Time-domain simulation of a guitar: Model and method. *J. Acoust. Soc. Am.*, 6(114):3368 – 3383, 2003.

[3] E. Bécache, P. Joly, and C. Tsogka. Eléments finis mixtes et condensation de masse en élastodynamique linéaire. (i) construction. *C.R. Acad. Sci. Paris*, t. 325, Série I:545–550, 1997.

[4] E. Bécache, P. Joly, and C. Tsogka. An analysis of new mixed finite elements for the approximation of wave propagation problems. *SINUM*, 37(4):1053–1084, 2000.

[5] E. Bécache, P. Joly, and C. Tsogka. Fictitious domains, mixed finite elements and perfectly matched layers for 2d elastic wave propagation. *J. of Comp. Acous*, 9(3):1175–1203, 2001.

[6] E. Bécache, P. Joly, and C. Tsogka. A new family of mixed finite elements for the linear elastodynamic problem. *SINUM*, 39(6):2109–2132, 2002.

[7] E. Bécache, J. Rodriguez, and C. Tsogka. Convergence results of the fictitious domain method for a mixed formulation of the wave equation with a neumann boundary condition. *Mathematical Modelling and Numerical Analysis(M2AN)*, 2009.

[8] J. P. Bérenger. A Perfectly Matched Layer for the Absorption of Electromagnetic Waves. *J. of Comp. Phys.*, 114:185–200, 1994.

[9] F. Collino, P. Joly, and F. Millot. Fictitious domain method for unsteady problems: Application to Electromagnetic scattering. *J.C.P*, 138(2):907–938, December 1997.

[10] F. Collino and C. Tsogka. Application of the PML Absorbing Layer Model to the Linear Elastodynamic Problem in Anisotropic Heteregeneous Media. *Geophysics*, 66(1):294–307, 2001.

[11] S. Garcès. *Application des méthodes de domaines fictifs à la modélisation des structures rayonnantes tridimensionnelles*. PhD thesis, 1998.

[12] V. Girault and R. Glowinski. Error analysis of a fictitious domain method applied to a Dirichlet problem. *Japan J. Indust. Appl. Math.*, 12(3):487–514, 1995.

[13] R. Glowinski, T.W. Pan, and J. Periaux. A fictitious domain method for Dirichlet problem and applications. *Comp. Meth. in Appl. Mech. and Eng.*, 111(3-4):283–303, 1994.

[14] Roland Glowinski and Yuri Kuznetsov. On the solution of the Dirichlet problem for linear elliptic operators by a distributed Lagrange multiplier method. *C. R. Acad. Sci. Paris Sér. I Math.*, 327(7):693–698, 1998.

[15] P. Grisvard. *Problmes aux limites dans les polygones. Mode d'emploi*. EDF.

[16] Erkki Heikkola, Yuri A. Kuznetsov, Pekka Neittaanmäki, and Jari Toivanen. Fictitious domain methods for the numerical solution of two-dimensional scattering problems. *J. Comput. Phys.*, 145(1):89–109, 1998.

[17] Erkki Heikkola, Tuomo Rossi, and Jari Toivanen. A domain embedding method for scattering problems with an absorbing boundary or a perfectly matched layer. *J. Comput. Acoust.*, 11(2):159–174, 2003. Medium-frequency acoustics.

[18] P. Joly and L. Rhaouti. Analyse numérique - Domaines fictifs, éléments finis H(div) et condition de Neumann : le problème de la condition inf-sup . *C.R. Acad. Sci. Paris*, 328, Série I(12):1225–1230, 1999.

[19] Yu. A. Kuznetsov. Fictitious component and domain decomposition methods for the solution of eigenvalue problems. In *Computing methods in applied sciences and engineering, VII (Versailles, 1985)*, pages 155–172. North-Holland, Amsterdam, 1986.

[20] J.C. Nédélec. A new family of mixed finite elements in $\mathbb{R}^3$. *Numer. Math.*, 50:57–81, 1986.

[21] L. Rhaouti. *Domaines fictifs pour la modélisation d'un probème d' interaction fluide-structure: simulation de la timbale*. PhD thesis, Paris IX, 1999.